Hindawi Publishing Corporation
Journal of Sensors
Volume 2009, Article ID 516850, 20 pages
doi:10.1155/2009/516850

Review Article

A Complex of the Electromagnetic Biosensors with a Nanowired Pickup

Rostyslav Sklyar

Verchratskogo st. 15-1, Lviv 79010, Ukraine

Correspondence should be addressed to Rostyslav Sklyar, sklyar@tsp.lviv.ua

Received 29 April 2009; Accepted 24 September 2009

Recommended by Joan Daniel Prades

The proposal to measure the biosignal values of different origins with advanced nanosensors of electromagnetic quantities is justified when allowing for superconducting abilities of the devices. They are composed in full-scale arrays. The said arrays can be both implantable into ionic channels of an organism and sheathed on the sources of the electromagnetic emanation. Nanowired head sensors function both in passive mode for picking up the biosignals and with additional excitation of a defined biomedium through the same head (in reverse). The designed variety of bio-nanosensors allow interfacing a variety of biosignals with the external systems, also with a possibility to control the exposure on an organism by artificially created signals. The calculated signals lies in the range of -5 to 5 V, $(7 \div 0) \cdot 10^{17}/\text{cm}^3$ molecules or magnetic beads, $2 \div 10$ pH, and stream speed $3 \cdot 10^{-3} \div 10^2$ m/s, flow $10^{-5} \div 10$ m/s, and haemoglobin concentration of $10^{30} \div 10^{24}$ molec/cm^3. The sensitivity of this micro- or nanoscope can be estimated as $H_J = 10^{-4}$ (A $\cdot$ m/$\sqrt{}$Hz) with SNR equal to 10^4. The sensitivity of an advanced first-order biogradiometer is equal to 3 fT/$\sqrt{}$Hz. The smallest resolvable change in magnetic moment detected by this system in the band 10 Hz is 1 fJ/T.

1. Introduction. The Nanowires Based Elements and Devices

Carbon nanocoils (CNCs), are a new type of promising nanomaterials. These have attracted considerable attention because of their potential applications, for example, parts for nano or micro-electromechanical systems, electromagnetic (EM) wave absorbers, reinforced composites, nanosolenoids, and field emission devices. Furthermore, the detailed analyses of the microscopic structures of the catalyst particles are very interesting subjects for future studies. These thin and highly crystallized multiwalled CNCs would find wide applications in new nanotechnology [1]. CNCs with nanometer-scale size are attracting much because of their peculiar helical morphology, aligned toward the electric field, and form a small aggregation of a CNC chain by the dipolar interaction of CNCs [2].

Self-assembled molecular nanowires (NWs), achieving four-level switching in a multiwire transistor and demonstrating their suitability for the production of multilogic devices, have been studied. Wires were composed of a single crystal, allowing good electrical transport with low resistivity. Field-effect transistors (FETs) with single- and doublewire channels were fabricated to give some indication of the potential application of the molecular wires. Appropriate molecular design and control of interfacial interactions lead to single crystalline wire growth with an extensive π-stacking motif. The single- and doublewire transistors were fabricated, successfully using needle probes to apply gate voltage [3]. With the latter, a double top gate configuration enabled independent control of the drain current through each wire and enabled modulation to four different values by turning gate voltage on and off. Resistivity measurements of an individual molecular wire indicate that the structural features are advantageous for electrical transport.

The first metal-semiconductor FET was fabricated with a self-assembled, planar gallium-arsenide NW channel (Figure 1). Compound semiconductor NWs, such as gallium arsenide, are especially desirable because of their better transport properties and versatile heterojunctions. The self-aligned orientation of the NWs is determined by the crystal structure of the substrate and certain growth parameters. By replacing the standard channel in a metal-semiconductor FET with one of planar NWs, the defect-free NW's electron

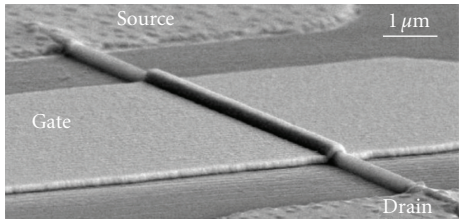

Figure 1: A scanning electron microscope image of self-assembled and self-aligned planar gallium arsenide NWs. © 2009 IEEE.

mobility became as high as the corresponding bulk value [4].

Treated NWs could serve as very sensitive toxin or pathogen detectors. Making NW detectors involves coating them with molecules that bind to certain target molecules, such as viruses or proteins. When a single target molecule attaches to the coating, the NW's conductivity changes. Detecting this electrical signal leads to sensors that are smaller, cheaper, and more sensitive than using current diagnostic chips, which rely on large microscopes to detect fluorescent molecules attached to the target molecule. The difficulty has been finding an easy way to integrate the NWs with electronics. To etch three rows of shallow rectangular wells on a silicon chip using an electric field might be simpler; each well is designed to hold a single NW. An electric field to the first row is applied—the field's strength is designed to vary along the row and deposit a solution of the first type of DNA-coated NW. Electrodes are deposited on their NW arrays, showing that an electrical connection to the wires is possible.

Short platinum nanowires already have been used in submicroscopic sensors and other applications. A method of making long (cm) Pt NWs of a few nanometers in diameter from electrospinning was described [5]. Those wires could be woven into the first self-supporting webs of pure platinum (Figure 2). By a process known as electrospinning, the platinum NWs long enough to construct the web are made.

Single-wall carbon nanotubes (SWNTs) are one of the most attractive materials in terms of both fundamental science and technology due to their unique character. SWNTs are also promising for building nanoscale electronic devices and microelectrodes [6]. In particular, carbon nanotube FETs (CNTFETs) are promising candidates for high-sensitive label-free biosensors due to their unique geometries with high surface-to-volume ratio. The detection of biomolecules such as DNA or proteins has been successfully performed using CNTFETs. High-performance local-electrolyte-gated CNTFETs, in which the channel conductance modulation effect is dominant in the switching, have been fabricated.

The top-gate CNTFETs with the ultrathin high k dielectrics by depositing the HfO_2 on DNA-functionalized SWCNTs have been fabricated with atomic layer deposition (ALD) technique (Figure 3) [7]. With the DNA functionalization, and the high performance nanotube-high k FETs, free of gate-leakage currents were reliably obtained with HfO_2 thickness down to 2-3 nm. The fabricated CNT-FETs could reliably achieve the subthreshold slope S = 60 mV/decade at room temperature.

Recently, organic thin-film FET (TF-FET) has been investigated for future device applications [8]. While much of this interest has focused on the operation of devices that utilize carbon nanotubes as their functional elements, a new type of C_{60} needle, or nanowhisker (NW) has recently been obtained by liquid-liquid interfacial precipitation (LLIP) (Figure 4).

The V_g dependences of I_{sd} are shown in Figure 5 for various conditions. The on/off ratio has decreased from 3 to 2 orders of magnitude after evacuation.

The lipid bilayer membranes have been incorporated into SiNW transistors by covering the NW with a continuous lipid bilayer shell that forms a barrier between the NW surface and solution species [9]. When this "shielded wire" structure incorporates transmembrane peptide pores, it enables ionic to electronic signal transduction by using voltage-gated and chemically gated ion transport through the membrane pores (Figure 6).

Double-gated silicon NW structures (DG-SiNW), where the position and/or type of the charge could be tuned within the NW by electric field, have been studied [9]. DG-NW structures have several beneficial properties, for example, the possibility to change the distribution of the charge could be used to increase the sensitivity of the sensor by pushing the charge towards the functionalized surface. In addition, the dynamic range of the sensor could be enhanced by tuning the sensitivity in a similar manner. Furthermore, the DG structures have also been proposed to be used as a velocity modulation transistor, which could act as a basic building block for ultrafast data processing purposes.

2. EM Bio-Nanosensor Arrays

New nanomaterial approaches aimed to modify surfaces have the potential to deliver a new generation of biosensors and bioelectronic devices for biomedical applications. They are anticipated to have improved performance over existing technologies. The integration of biomolecules with CNTs enables the use of such hybrid systems as electrochemical biosensors (enzyme electrodes, immunosensors, or DNA sensors) and active FETs. A method to functionalize SWCNTs in an FET device for the selective detection of heavy-metal ions with the signal transduction mechanism has been reported [10].

Carbon nanotubes have a range of unique properties, not the least of which are their electronic properties and their size. The combination of these two important properties has seen them investigated extensively in the last few years in bioelectronic devices, such as biosensors. The applications of carbon nanotubes in bioelectronics have resulted in carbon nanotubes being used as nanoscale electrode elements. They are plugged into biological molecules, as electronic elements upon which biomolecular interactions can be monitored and as platforms upon which biomolecules can be attached.

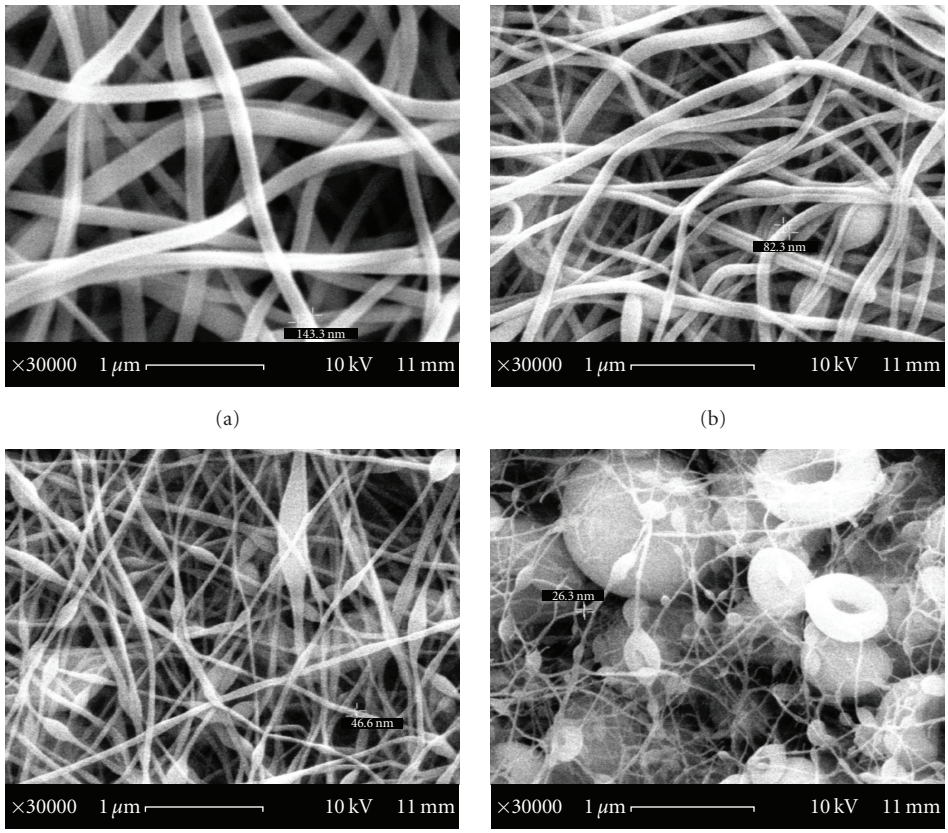

Figure 2: The longest platinum NWs ever made. Reprinted with permission from [5]. Copyright 2009 American Chemical Society.

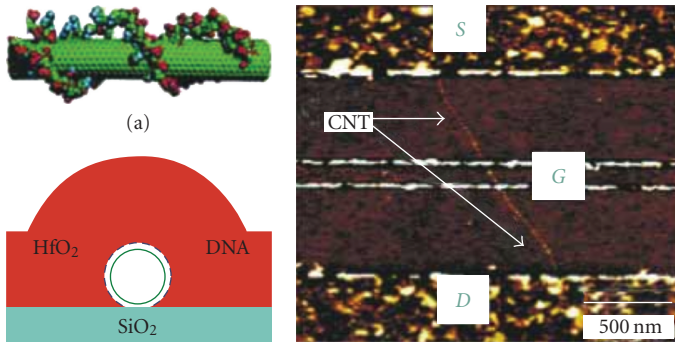

Figure 3: The CNTFETs fabricated by depositing the HfO_2 on DNA-functionalized SWCNTs with atomic layer deposition (ALD) technique: (a) Schematic of a DNA coated SWNT, (b) Cross-sectional view of HfO_2 (~3 nm by ALD) conformally deposited on a DNA functionalized nanotube lying on a SiO_2 substrate, (c) Atomic force microscopy (AFM) image of a high k SWNT FET with top-gate (G), underlapping source (S), and drain (D). Reprinted with permission from [7]. Copyright 2006 American Chemical Society.

Real sensors detect unwanted signals, referred to as noise. Noise is broadly divided into two categories—uncorrelated noise and correlated noise. Uncorrelated noise is induced by the sensors, thermal fluctuations in conductors (Johnson noise), or by thermal fluctuations in magnetic susceptibility of nearby materials within shielded parts of the sensors. Correlated noise which appears in all or most of the sensors can be due to environmental disturbances such as moving vehicles, elevators, and power lines, also from near-field biological disturbances such as the magnetic field of the heart and muscles or displacement of the body tissue in the local magnetic field. Even unwanted brain signals (i.e., signals from parts of the brain that are of no interest to a study) can be considered to be noise. We refer to this as "brain noise."

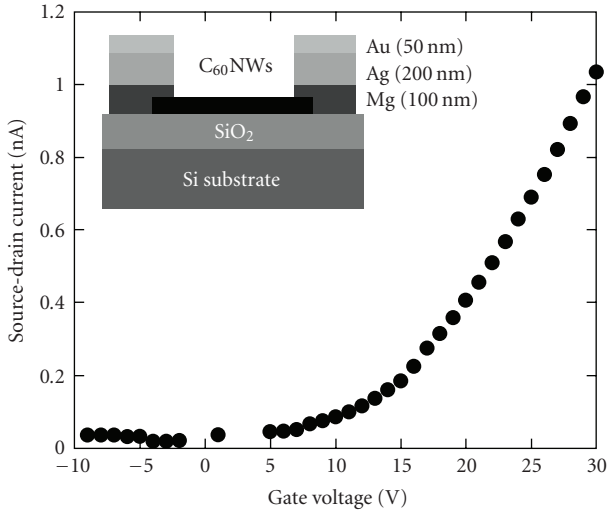

FIGURE 4: The I_{sd}-V_g (a) and the I_{sd}-V_{sd} (b) characteristics of a C_{60} NW-FET are shown in the case of top-contact Mg electrodes. The inset in (a) shows a schematic cross-sectional view of the sample. Reprinted with permission from [8].

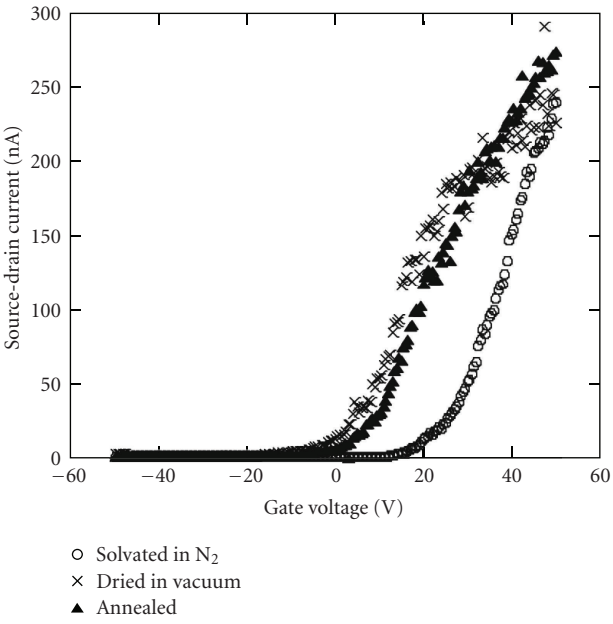

FIGURE 5: The I_{sd}-V_g characteristics for a solvated (chlorobenzene) C_{60} NW with bottom-contact Au electrodes. Reprinted with permission from [8].

In addition, correlated noise can be caused by Johnson noise and magnetic susceptibility of nearby materials which are exposed to all flux transformers (e.g., dewar materials) [11].

Calculations of sensor arrays were performed with the primary sensor flux transformer sites distributed uniformly on a spherical sensor shell, extending from the vertex to a maximum angle max, as shown in Figure 7(a). The radial magnetometers and gradiometers occupy one site each (Figures 7(b) and 7(c)), there are two orthogonal planar gradiometers at each site (Figure 7(d)) and there are three orthogonal magnetometers at each site for vector magnetometers.

2.1. NWs-Based Two-Way Transducing of the Biosignals. Among the variety of the presented FET devices, there are a majority of them, mainly modifications of nanoFETs, which allow simultaneous processing of a number of the biosignals (BSs) directly or from the pickup coil (PC) [12]. There are two factors that make simultaneous processing possible. First of all, the sizes of nanoFETs and nanoPCs are in the same order as the transmitting substances of BSs, such as axons, neurons, and the DNA spiral. Secondly, the crossed-NW FET array is, in itself, multi-input. The remaining parts of FET devices are applicable for serial connection to the said mediums. In addition, some of these FETs can be arranged in the chain in order to transduce the BSs into different physical and chemical quantities and vice versa [13].

Superconducting NWs are unusual in their newer show zero resistance, although resistance does exponentially decrease upon cooling. A new class of metallic devices based on DNA molecules is promising due to the self-assembly properties of DNA. As the resistance of the devices is controlled by the spatial profile of superconducting phase within the leads, there is the potential for applications. These include local magnetometry (as is widely done with conventional SQUID) and the imaging of phase profiles created by supercurrents—in essence a superconducting phase gradiometer.

Creative integration of microchip technologies and nanostructures is feasible. By tuning the dielectrophoretic frequency within a microdevice, nanoparticles can be manipulated with the same precision as cells because a one-to-one correspondence exists between a given alternating current frequency and a nanoparticle interaction or biological event. Multiple biological events could be probed simultaneously provided that their corresponding frequencies are distinct. Alternatively, functionalized nanoposts can be used to impale cells and relay information from the cell interior to nanoelectronic circuits. The report shows how the scientists fabricate FETs from CNT with the precise electrical properties and any variable band-gap desired. In parallel studies of CNT, researchers have been working to improve the electrical characteristics of individual nanotube transistors.

2.2. Measuring of the Excited EM Signals—Biosusceptometer and Nano-Microscope. The main difficulties in the measurement of biosusceptibility are irregular shapes of the investigated objects, which are difficult to be formalized, and this susceptibility is inhomogeneous. Following the measurement in vivo the NWPC should be maximally penetrative and flexible to follow the object's form and miniature to have the high resolution ability. Simultaneously, the angle between the outside-magnetized coil and an inside NWPC should be adjusted due to the amplification of the signal from some particular areas. Also to raise the sensitivity, laid down in vivo areas, it is necessary to use the Helmholtz coils for the creation of the laminar magnetic fields (MFs).

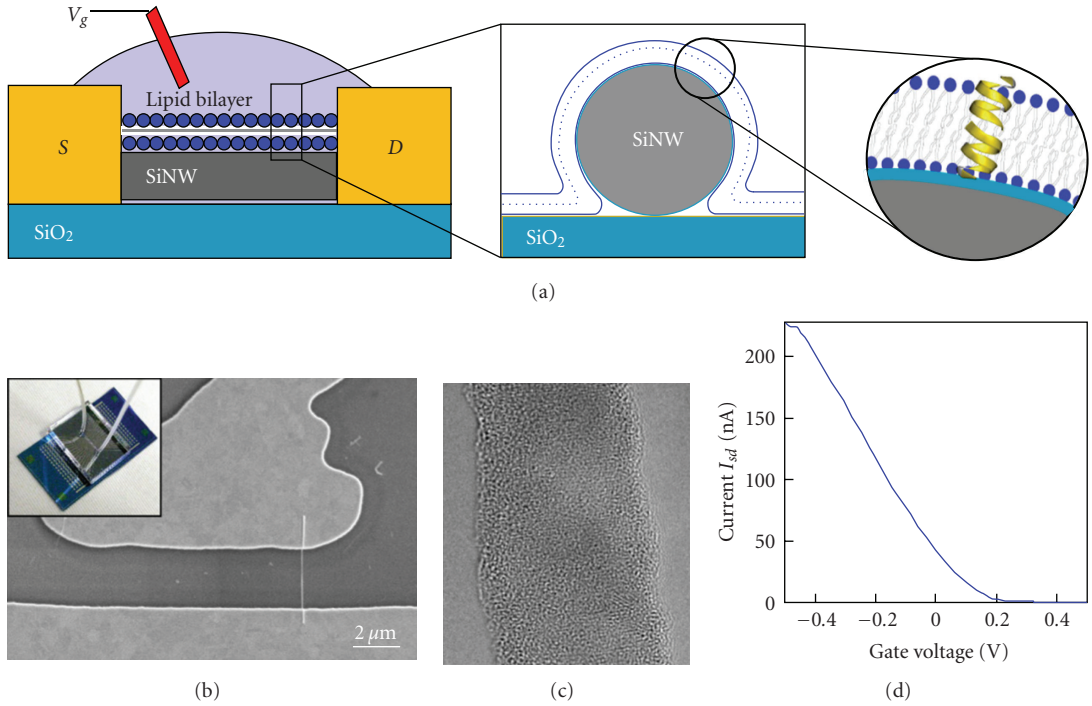

Figure 6: Bionanoelectronic devices incorporating lipid-coated SiNWs [9]. (a) Device schematics showing an NW connected to microfabricated source (S) and drain (D) electrodes. (Insets) The configuration of the lipid bilayer and a pore channel placed in the bilayer membrane. (b) An SEM micrograph of the NW transistor showing an NW bridging the source and drain electrodes. (Inset) A photograph of the device chip covered with a PDMS flow channel. (c) TEM micrograph of the as-synthesized SiNW. (d) A typical IV characteristic of the SiNW transistor in fluid. Copyright 2009 National Academy of Sciences, U.S.A.

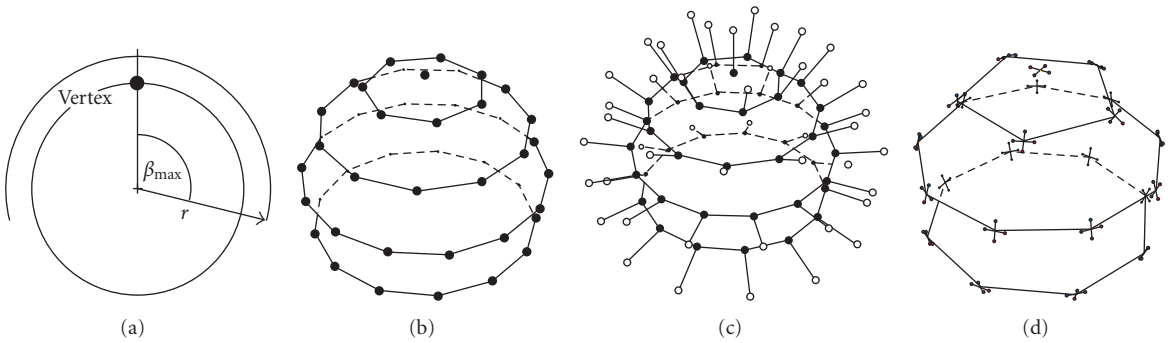

Figure 7: Examples of sensor arrays. To make the figure easier to comprehend, all sensor arrays are shown with only 46 channels. For clarity, the sites corresponding to the same angle from the vertex are interconnected by lines. (a) Geometry of the sensor shell. Sensors are uniformly distributed on a spherical surface (with radius r) extending from vertex to an angle max; (b) radial magnetometers; (c) radial gradiometers, sensing coils are indicated by solid dots and the more distant coils by empty dots. The gradiometer baseline is shown by a line connecting the corresponding gradiometer coils; (d) planar gradiometers. At each site there are two orthogonal planar gradiometers. Reprinted with permission from [11], IOP Publishing Ltd.

Since the field and spatial resolution are highly diminished as the distance between the sample and the sensor increases, the key to this technique is to bring the sensor (held in at cryogenic temperatures) as close as possible to the sample. It has been shown that the best combination of spatial resolution and field sensitivity for a specific SQUID geometry occurs when the diameter of PC is approximately equal to the sample-to-sensor distance [14]. These systems do not provide the spatial resolution necessary to study the generation of the magnetic activity or injury currents at tissue and cellular scales. In excitable tissue, extracellular potentials, transmembrane potentials, or action currents are interrelated. The extracellular potentials are typically recorded using microneedle arrays. However, the insertion of microneedles influences the measurement results and is impractical to achieve submillimeter (nano) special resolution. The approach to record the action currents using SQUID microscopy allows us to obtain more detailed

information on the generation of the magnetocardiogram (MCG). High-resolution biomagnetic (BM) imaging provides insights that will improve existing mathematical models of biological tissue.

Taking into account all the described requirements it is advancing the configuration of the measuring system. The part of living object is excited by a quasiDC or AC magnetic field; $H(r)$, generated by Helmholtz coils, is penetrated to the investigating subject. The magnetization $M(r)$ of an organ or tissue is detected by the in vivo NWPC of induction sensor (IS) that creates a corresponding output voltage U_{out}. PC could be handled in any direction of the subject's irregular form by a biochemically inert rod or manipulator. For the defined values of the IS's circuit, $K_{\text{Hl}} = 10\ (1/\text{m})$, and exiting frequency 10 Hz, $\chi(r)$ will be equal to $\chi(r) = 5 \cdot 10^4 \cdot V_{\text{GS}}/U_{\text{in}}$.

For the typical reference of an NWPC's radius to the radius of wire as the value of $a/c = 100$, the previous sensitivity of biogradiometer is defined as: $S_H = 4 \cdot 10^{-6} \cdot \eta E_J / a^3$. For the NWPC's radius 0.001 (m), the sensitivity of an advanced first-order biogradiometer is equal to: $3\ \text{fT}/\sqrt{\text{Hz}}$. The smallest resolvable change in magnetic moment detected by this system in the band 10 Hz is 1 fJ/T.

A new design for scanning or sounding nano-microscope combines a simple mechanical arrangement with NWPC connected to SuFET [15]. The microwave imaging process is shown on a prototype sample: a normal conducting ring of self-inductance L_i and resistance R_i. The quantity L_0 is the exciting coil (EC)/PC (NWEC/PC) self-inductance, and MI_i represents the magnetic coupling of the PC through a mutual inductance M to an external circuit carrying a current I_i in a tissue. If $\omega_T \gg R_i L_i$, then R_i may be ignored and $I_i(\omega_T) \approx -I_j(\omega_T)M/L_i$. Thus, by monitoring the change in $\Delta I_j(\omega_T)$ as a function of NWPC position, we make use of the factor M/L_i dynamics of the tissue to obtain a micro- or nanowave screening image.

The sensitivity of this instrument H_J can be estimated by considering the noise source I_{NJ} of SuFET accordingly. The digital value of H_J for PC with the diameter of 0.1 μm and inductance 1 μH, and $I_{\text{NJ}} = 10^{-11}\,(\text{A} \cdot \text{Hz})$ is equal to: $H_J = I_{\text{NJ}} L/\mu_0 S_{\text{eq}} = 10^{-4}\,(\text{A} \cdot \text{m}/\sqrt{\text{Hz}})$. This means that with an SIM exciting signal $H_{\text{sign}} = (V_{\text{DS}}/2\text{-}V_{\text{GS}})/\mu_0 S_{\text{eq}} \omega_T = (V_{\text{DS}}/2\text{-}V_{\text{GS}}) \cdot 10^3 \approx 1\,(\text{A} \cdot \text{m})$, a magnetic SNR in a band less than 10 Hz will be: $H_{\text{sign}}/H_{\text{R}}(\Delta 10\,\text{Hz}) = (V_{\text{DS}}/2\text{-}V_{\text{GS}})/\ I_{\text{NJ}} L \omega_T$. For the said values, SNR of the described NMSC will be equal to $H_{\text{SNR}} = (V_{\text{DS}}/2\text{-}V_{\text{GS}}) \cdot 10^7 \approx 10^4$. Typically our magnetic images are taken at about 8 pixels/s.

2.3. Determination of the Density of Ferromagnetic Particles in the Volume Flow. The value of the magnetic permeability μ in blood flow, Figure 8, should vary. That is why this variation will influence the measuring partial of MF: both B and strength H. It means that the variation of the density of ferro- or paramagnetic particles into the stream can be determined when the speed of a stream is constant. To measure all three directions of blood velocity provides the ability to visualize two- or even three-directional blood flow patterns. It also promises a noninvasive quantification of the mechanical energy losses of blood as it flows through the connection. New rapid acquisition sequences show accuracy in quantifying flow [16].

This technique can be explained using the example of the advancing counting/measuring device of hemoglobinum level in bloodflow (BF) [17]. This level is influenced by the paramagnetic susceptibility of the flow due to variation in the density of ferrum molecules into it. Such variations $\Delta H = H - H_{\text{fl}}$ in the ambient MF H are absorbed by a solenoidal PC which embraces the BF (Figure 19). As a result the output voltage U_{out} of IS defines both the absolute value of hemoglobinum content and variations of its density in respect to some optimal value.

The magnetic permeability of the medium (in this case BF) is defined as

$$\mu = 1 + \chi. \tag{1}$$

The classical value of paramagnetic susceptibility derives as

$$\chi_{\text{cl}} = \frac{NM_a^2}{3kT}, \tag{2}$$

where k: Boltzmann's constant; T: absolute temperature; M_a: spontaneous magnetization of ferrum molecules.

This gives us the possibility of defining the magnetic susceptibility of blood according to the following formula:

$$\mu = 1 + \chi_{\text{cl}} = 1 + \frac{NM_a^2}{3kT} = 1 + 225\frac{NM_B^2}{kT}, \tag{3}$$

where $M_B = 1.165 \cdot 10^{-29}\ (\text{Wb}\cdot\text{m})$ is a magneton of Bohr.

Employing some substances as a core of PC is expected to define an effective magnetic permeability μ_{ef} of the formed physical body. As big veins and arteries are possible to consider as long cylinders, in consequence for them the following expression is valid:

$$\mu_{\text{ef}} = \frac{\mu\mu_{\text{dm}}}{\mu + \mu_{\text{dm}} - 1}, \qquad \mu_{\text{dm}} = \frac{m^2}{\ln 2m - 1}, \tag{4}$$

where m is a ratio of the length of a cylinder to the diameter.

As a result, a formula for the PC's core which is formed by big BF vessels can be written down as

$$\mu_{\text{ef}} = \frac{m^2(kT + 225NM_B^2)}{m^2 kT + 225(\ln(2m) - 1)NM_B^2}. \tag{5}$$

An analysis of this formula provides evidence that requirement $\mu_{\text{ef}} \gg 1$ will be satisfied under condition $m^2 \gg \ln 2m - 1$, which for long cores with $m \gg 1$ will always be true. That is why we acquire a ferromagnetic core in the form of a BF, which gives us the chance to create on its bases an IS from one of five modifications. The input voltage of these ISs is defined by the known equations and stand duty as measured quantity which is linearly connected with change μ_{ef} of PC, defined for a blood bed by (5).

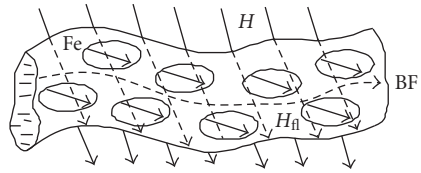

Figure 8: Variation H_{fl} of an ambient MF H in a BF secondary to the changes of ferrum molecules' density.

3. An EM Transistor/Memristor (EMTM) Device and Its Connection into Arrays by Nanowires

Implantable neural probes are generally preferred to have a minimum footprint as possible to minimize neural damage and to facilitate easy entry and movement through the brain tissue. To date, a wide range of neural electrodes have been used in basic neuroscience and neural prosthetic research (brain machine interfaces) starting with the early electrolyte-filled micropipettes [18]. More recently, polymeric micro-probes have received a great deal of attention due to their simple fabrication process, flexibility, and biocompatibility.

Alternatively, a SuFET based neurotransducer with carbon nanotubes (CNT) or pickup coil (PC) kind of input circuit for the nerve and neuron impulse has been designed. A nanoSuFET with a high-temperature superconducting channel is introduced into the nerve fibre or brain tissue for transducing their signals in both directions [13].

A further step should be synthesis of the said two methods in order to develop the external (nonimplantable) nano-bio-sensing arrays. Human beings from which EM signals are to be extracted are attached with an EM sensor and the raw EM signal is acquired. The EM sensors are surface PCs, which are used in a regular configuration, where PCs with a small distance between each other are positioned within the helmet type surface to pick up the local signals within the place of interest.

The term "magnetoencephalography (MEG) sensor array means the collection of EMTMs [19]. Rejection of environmental noise can be improved by measuring a magnetic field difference, rather than the field itself. Such flux transformers are referred to as gradiometers (i.e., the field difference approximates a component of the field gradient tensor) [3]. The radial gradiometer detects the radial gradient of a radial MF (radial with respect to the surface of the head).

The 20 cm^2 array for sheathing of the brain consists of 40 thousands EMTs which could be produced by printed electronics processes. These elements are set out into the square or rectangular matrices A and take part in further mathematical operations [20]. Control (and interaction) signals can be both in the current and voltage forms to create MF or EF, respectively. Signal contribution corresponding to a dipole of a specified rms amplitude and at a specified position within the model sphere was added to the noise covariance matrix and the resulting covariance matrix was used to compute SAM depth profiles.

The problem of sensing the EM signal for amplification/switching/memory with a speed of light in a single solid-state device (EMTM) has been advanced [20]. The said problem in the advanced method is solved by application of ferroelectric or ferro EM (FE or FEM) crystals which are controlled by an electric or magnetic fields (EF or MF), respectively. The device for controlling (amplifying, switching) of a magnetic flux in the processing crystal is designed with an application of ferromagnetic material with a unique fashion dependence between its magnetic permeability and the strength of MF. Also controlling the device by both an electric and a magnetic field allows matching it with the previous stages.

On a basis of the acquired equations, which are defining the nonlinear characteristics of the passive elements in an EMTM circuit, it is possible to define the in-out dependence for a control coil [21]. A matrix equation for the output value of MF takes some form, which after substitution to the final signal processing matrix for a control e. g. f. element with the internal resistance is resolved by analytical or digital methods.

A memristor is a 2-terminal thin-film electrical circuit element that changes its resistance depending on the total amount of charge that flows through the device. This property arises naturally in systems for which the electronic and dopant equations of motion in a semiconductor are coupled in the presence of an applied electric field. Our EMTM device can expand this ability by an applied MF.

The first feasibility demonstration for the integration and operation of nanoscale memristor crossbars with monolithic on-chip FETs has been presented [22]. In this case, the memristors were simply used as 2-state switches (ON and OFF, or switch closed and opened, respectively) rather than dynamic nonlinear analog device to perform wired-logic functions and signal routing for the FETs. The FETs were operated in either follower or inverter/amplifier modes to illustrate either signal restoration or fast operation of a compound binary logic function, "(A AND B) OR (C AND D)," also, written using the Boolean algebra representation as AD CD, in which logical AND is represented by multiplication and OR by addition. These exercises were the prelude to the primary experiment, which was the conditional programming of a nanomemristor within a crossbar array by the hybrid circuit. A proof-of-principles provides validation that the same devices as EMTMs in a nanoscale circuit can be configured to act as logic, signal routing, and memory, and the circuit can even reconfigure itself.

Figure 9 displays in various colors the NWs in the crossbar selected from those that were determined to be good and the conductance map for the programmed-ON memristors. The gray-scale squares display the current through the individual memristors upon the application of a test voltage of 500-mV bias.

Figure 10 shows the time dependence of the 4 MF pulse traces V_A to V_D acting as the inputs to the compound logic operation. The speed of the circuit was actually limited by the load on the output transistor, which had to charge the parasitic capacitance of the measurement cabling.

The processing matrix is a subject for control by BM field according to a novel method [23]. A general hybrid architectural approach named FPNI (field-programmable

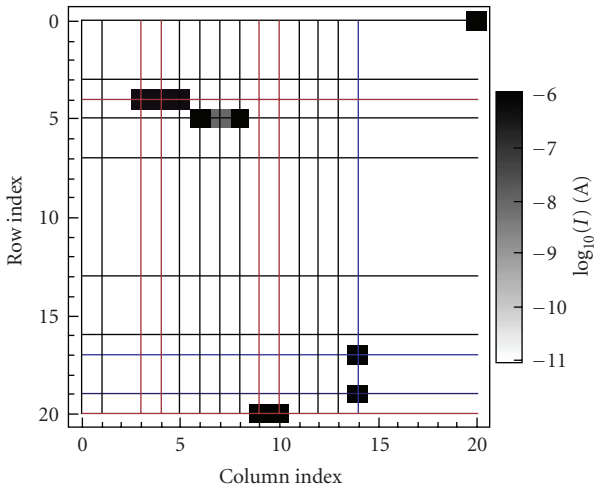

FIGURE 9: Map of the conductance of the memristors in the crossbar [22]. Copyright 2009 National Academy of Sciences, U.S.A. The straight lines represent the continuous NWs, and their colors correspond to those of the circuit in *A*. The broken NWs are the missing black lines in the array. The squares display the logarithm of the current through memristor at a 0.5-V bias.

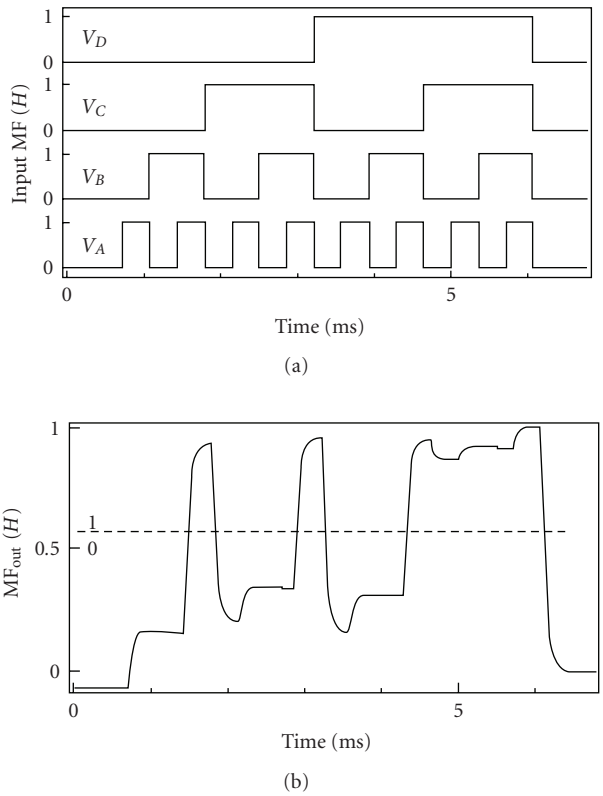

FIGURE 10: Operation of the logic circuit. (a) The time sequence of the input MF pulses used to represent the logic values 1 and 0 for the 4 inputs *A* through *D*, and (b) the output MF versus time that represents the 16 outcomes from the 4-input compound logic operation ABCD [22]. Copyright 2009 National Academy of Sciences, U.S.A.

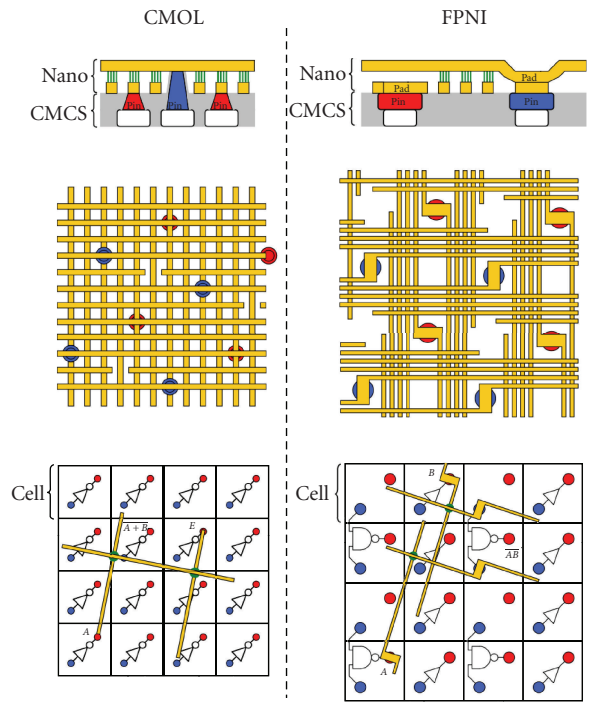

FIGURE 11: Schematic diagrams of hybrid circuits. The CMOL (left column) places an NW crossbar on top of a sea of CMOS inverters. The FPNI (right column) places a sparser crossbar on top of CMOS gates and buffers. Reprinted with permission from [23], IOP Publishing Ltd.

NW interconnect) that trades off speed, density, and defect-tolerance of CMOL (CMOS/molecular hybrid) in exchange for easier fabrication, lower power dissipation, and greater freedom in the selection of nanodevices in the crossbar junctions has been presented.

Figure 11 compares the geometry of nanowires, pins, and underlying CMOS for the two approaches. The CMOL (left column of Figure 11) assumes a sea of inverters regularly connected to pins on the surface of the silicon. Selected junctions (shown in green in the bottom panel) are configured as nonlinear resistors to implement wired-OR logic (in conjunction with a pull-down transistor in the CMOS), with the CMOS inverters providing gain and inversion. The FPNI (right column of Figure 11) assumes a sea of logic gates, buffers, and other components in the CMOS layer, and uses the NWs only for the interconnect. Selected junctions (green, bottom panel) are configured as resistors to interconnect the underlying logic. As the pin size and alignment error approach zero, the CMOL NW layout emerges as a special case of FPNI.

4. Using of the MHD and EGD Effects for Measuring of the Volume and Speed of Breath

Non-contact passive measuring of the volume of substances and tissues is possible by using the IS with solenoidal and/or toroidal NWPCs which will embrace the flow [17]. These coil(s) can be both room temperature and superconducting

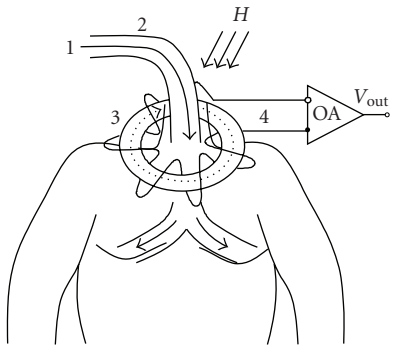

Figure 12: The stream of airflow 1 through trachea 2 generating vortical MF H_{fl} 3 which is picked up by the room temperature NWPC 4.

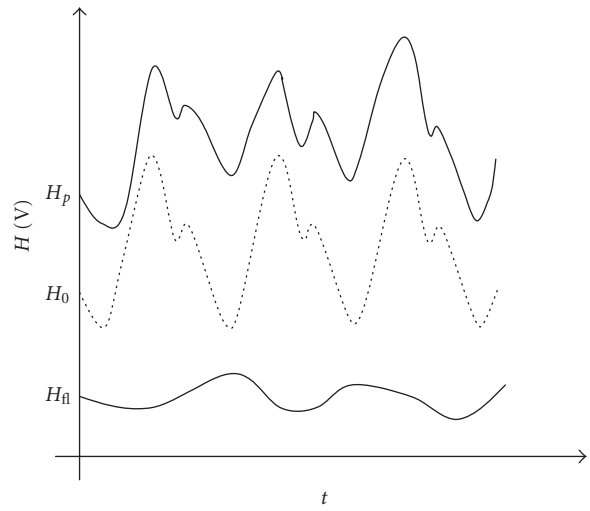

Figure 13: A result of subtraction H_{fl} of the external natural MF H_0 from the field immediately around the trachea H_p.

with connection to either common or superconducting FET. The measured quantities are (1) vortical MF of gasiform stream for the toroidal NWPC and (2) variation of the surrounding (natural) MF according to the magnetohydrodynamical (MGD) effect for the solenoidal PC. Microfluidic sensors promise detection of very low concentrations of analytes in volumes on the nanolitre scale.

4.1. Non-Contact Bioflowmeter of Gaseous or Friable Substances. Taking into account the said considerations, it is necessary to lay down the fundamentals of non-contact passive flowmeters (FMs). It is based on the effect of creating the vortical MF by ionized particles of the substances. This MF is transduced into the measurable voltage by the torus-like NWPC of IS.

There are a variety of MF sensors/transducers including two passive ones of high sensitivity: IS and SQUID devices. Non-contact passive measuring of the said substances and tissues is possible by using the induction sensor with solenoidal and/or toroidal NWPCs which will embrace the flow [17]. These coil(s) can be both room temperature and superconducting with connection to either common or SuFET. The measured quantities are (1) vortical MF of gasiform stream for the toroidal PC (Figure 12) and (2) variation of the surrounding (natural) MF according to the magnetohydrodynamical (MGD) effect for the solenoidal PC (Figure 6).

Measured MF interferes with the surrounding one. The variations of measured MF strength H_{fl} 1 of the stream (Figure 12) or flow (Figure 8) are a result of subtraction (Figure 13):

$$H_{fl} = H_p - H_0, \tag{6}$$

which corresponds linearly to the difference of the respective output voltages of the transducer.

The method of measuring the volume flow of liquids and gaseous or friable substances is by defining their interaction with only ambient natural MF. The first device based on this method is a passive and non-contact FM of gaseous or friable substances which includes a resistive or superconducting torus-like PC of an IS which is PC-placed around the jet-flow. As a result of this arrangement, the head transducer is considerably simplified. Since, it is the absence of introducing a high EM feld into the measured medium. The absence of mechanical interaction with flowing substances increases the reliability and life-span of the device. On the other hand, they completely retain the characteristics and composition of the flow components. Thus, the employment of a spontaneous MF causes the reduction of energy consumption to occur.

As a result of this arrangement, the measuring device is setting up without a failure of the vessels and interruption in their functioning. The absence of a measuring device or any moving members will considerably raise the safety factor in service due to the isolation of the flows from potentially combustible substances. It also gives us the chance to avoid any influence on the measuring substance, including the danger of changing its chemical or physical composition.

4.2. Bioflowmeter of Breathing Gases. According to pneumography the duration and frequency of breathing are defined according to changes in the speed/volume of air/gas flow.

One of the main mechanisms of gases ionization is their interaction with the surface of the solid body, that is, surface ionization. Such interaction arouses an electrogaseodynamical flow (Figure 13):

$$I = q_0 u_0 \pi h_i^2, \tag{7}$$

where q_0: the density of an electrical charge; u_0: the dimensionless speed of a gas flow; h_i: the radius of an electrogaseodynamical jet.

In such cases the MF strength on the distance r from the flow's edge is

$$\Delta H = \frac{I}{2\pi r}. \tag{8}$$

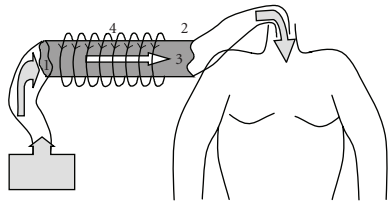

Figure 14: The gasiform or friable substances 1 which are ionized in consequence of interaction with the internal solid surface of a tube 2. The formed electro-gaseodynamical jet 3 induce the vortical MF 4.

As a result we have an equation:

$$\Delta H = \frac{q_0 u_0 h_i^2}{2r}, \tag{9}$$

where the swing of ΔH will follow the speed and frequency of breath.

This flow is absorbed by the torus-like PC of IS. It is necessary to notice, that an acquired value of MF strength will be generated outside the tube only when it is made of paramagnetic material. In the case of diamagnetical, and especially ferromagnetical metal or alloy, the measurement of some residual values occurs.

4.3. The Plethysmography Diagnostics. Plethysmography is the method for registering the changes in body volume or its parts. A special kind is a body plethysmography which has been applied for investigation of an external breathing and volume speed of a bloodflow (BF).

The first method was realized in the previous paragraphs 1 and 2. The second one is an FM of liquids and organic tissues (blood) or a counter of the ferromagnetic particles into this mediums, it consists of the same IS but with a solenoidal-shape PC (Figure 14).

Because of low Reynolds numbers, laminar flow is usually assumed. However, either by design or unintentionally, the flow characteristic in small channels is often altered (e.g., by surface interactions, viscous and diffusional effects, or electrical potentials). Therefore, its prediction is not always straightforward. Currently, most flow measurements rely on optical detection of markers, requiring the injection of tracers and transparent devices [24].

The use of nanotube-based (CNT) sensors will avoid problems associated with the current, and much larger implantable sensors, which can cause inflammation. The devices can be administered transdermally. CNT chemical sensors for liquids can be used for blood analysis. CNTs can also be used as flow sensors, when the flow of a liquid or bundles induces a voltage in the direction of flow. Flow sensors can also be used for precise measurements of gases utilized by respiratory apparatuses during surgery and automatic calculation of medical treatment fees [25] (Figure 15).

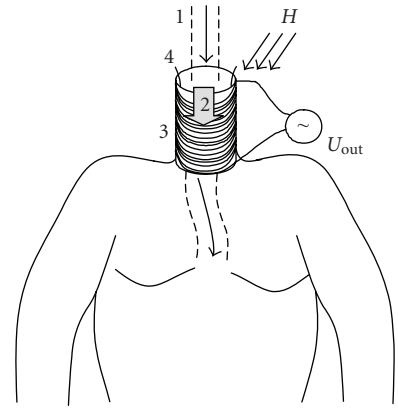

Figure 15: The originated in the bloodflow 1 partial H_{fl} 2 of the external natural MF H which is received by solenoidal PC 3, which is wrapped around the throat 4 of the ordinary or superconducting transducer.

For the liquid that moves between two nonconducting walls in the direction of this motion, the partial of the MF induction is arised [18],

$$B_x = B_0 R_M \frac{sh(Mz/L_0) - (z/L_0)shM}{MchM - shM}, \tag{10}$$

where B_0: the value of an ambient MF induction, which is perpendicular to the flow; L_0: a characteristic length; Z: the centre of a flow, and $z = \pm L_0$—the interval to the walls; R_m: the magnetic Reynold's number; and

$$M = B_0 L_0 \sqrt{\left(\frac{\sigma}{\rho\nu}\right)}, \tag{11}$$

where σ: a conductivity; ρ: a density; ν: the kinematic viscosity.

An equation for R_m is written

$$R_m = \frac{V_0 L_0}{\eta}, \tag{12}$$

where V_0: a characteristic velocity, which is comparable with an actual speed; $\eta = 1/\mu\sigma$—the factor of MF diffusion.

It is possible to count/register the changes of the volumes by summation of the momentum, relative to B_0, values of B_x (MF strength) without having contact with them:

$$\Delta V_n = \begin{Bmatrix} \sum_{i=1}^{n} (B_0 \pm B_x^+) \\ \sum_{i=1}^{n} (B_0 \pm B_x^-) \end{Bmatrix}, \tag{13}$$

where opposite directions of the flows are defined by B_x^+ and B_x^- (Figure 16).

The performance of IS of volume movement of these liquid substances and tissues laid down on measuring the variations of ambient MF strength will cause to pull it along with a moving medium which the strength crosses. Moreover, the gradiometrical configuration connection of PCs makes it possible to define the direction of the flow ($B_0 - B_x > 0$ or < 0) and the dynamic nature of its pulsations ($B_0 - B_x >$ or $< B_0 - B_x$).

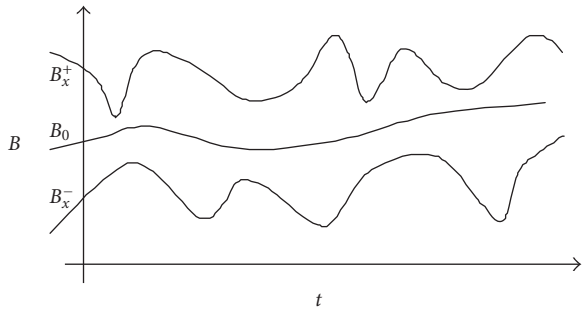

Figure 16: A dynamical difference of ambient MF changes between two places of artery or vain.

5. *n*-NWPCs Arrays for the BEM and Mechanical Sensors

A BM sensing array consists of primary sensors and, optionally, reference sensors. Primary sensors use flux transformers located in a close proximity to the scalp surface, where they couple to the brain's MF. The reference sensors are used to subtract the environmental noise from the primary sensor outputs. Several variations in primary flux transformer design, commonly used in multichannel BM systems, are shown in Figure 17 [11]. The flux transformer design dictates its relative sensitivity to near and distant sources. Thus, the primary flux transformers can, in addition to detecting the brain signals, also provide various degrees of the environmental noise rejection. Flux transformers illustrated in Figures 17(a)–17(c) are magnetometers. These devices have the highest sensitivity to both near- and far-field sources. Thus, they do not reduce the environmental noise (and must rely solely on the references or other techniques for the noise cancellation).

The examples shown in Figures 17(d)–17(f) are first-order hardware gradiometers (differential magnetometers). These provide reduced sensitivity to distant sources of environmental noise, while retaining good sensitivity to signals generated by the brain. Hardware gradiometers may also require supplemental noise cancellation.

Such a magnetometer can be rotated by 90°, as in Figure 17(b), to detect a tangential component relative to the scalp. It is then referred to as a tangential magnetometer. Note that the mean distance of the tangential magnetometer centre from the scalp surface is necessarily larger than that of a radial magnetometer. Three magnetometers, orthogonal to one another, can be combined to form a vector magnetometer, as in Figure 17(c).

Rejection of environmental noise (i.e., from distant sources) can be improved by measuring an MF difference, rather than the field itself. Such flux transformers are referred to as gradiometers (i.e., the field difference approximates a component of the field gradient tensor). A first-order radial gradiometer, Figure 17(d), consists of two axially displaced magnetometer loops, wound in opposing sense from a common NW that is connected to the SuFET device. The distance between the two loops is referred to as the gradiometer baseline. The radial gradiometer detects the radial gradient of a radial MF (radial with respect to the surface of the head).

The complete flux transformer optimization should also take into consideration the NWPC diameters. Since these diameters are smaller than the coil distances from the brain sources, the differences between the brain signals detected by the pozint or finite diameter coils are small (several per cent).

Gradiometers can also be configured to detect radial gradient of the tangential magnetic field, as illustrated in Figure 17(e). Two orthogonals "tangential radial gradiometers" and one "radial gradiometer" can be combined to form a first-order gradiometer equivalent of the vector magnetometer. Two radial magnetometers with opposite polarity can be connected together to form planar gradiometers, Figure 17(f) [21]. Such devices detect tangential gradient of the radial field, and two gradiometers are usually used at each site to detect two orthogonal planar gradients.

In general, the various first-order gradiometers discussed above measure one component of a first gradient tensor (which has nine components, of which five are linearly independent). Furthermore, by connecting combinations of gradiometers in opposition (either in hardware or in software), it is possible to create higher-order gradiometers.

Wire-wound gradiometers are the most conventional of the three. The NWPCs of wire-wound gradiometers are wound in opposition and balanced so that a uniform field can link the zero net flux. Wire-wound gradiometers are basically made of NW. These types of gradiometers are easy to fabricate and are commercially available for BM systems. As a result, a new type of wire-wound gradiometer based on a low-T_c SQUID with a high SNR as well as a wide dynamic range has been introduced [26]. Its properties in terms of signal intensity and the noise-reduction ratio (NRR), compared with conventional wire-wound gradiometers, were also discussed.

5.1. SIM with the Nanowire PCs for n-Axial MF Transducing. It is an attempt to generalize the current knowledge of passive magnetic field transducers and to incorporate elements of both designs in order to find a way to improve their performance data. By creating, in theory, a combined transducer, superconducting induction magnetometer (SIM) has been made [27]. The superconducting FET (SuFET) is incorporated into a wide-band BM field sensor device in order to acquire an ultimate sensitivity. The proposed magnetometer circuit consists of both room temperature or cooled (up to superconductive) NWPC and a SuFET. As a result, we achieve a magnetometer using a room temperature sensing (pickup, head) nanocoil, which has the possibility of further cooling together with a SuFET based preamplifier, which has a superconducting input.

The restricting conditions are $I_{\mathrm{NWPC}} \leq I_0$ (close but less) and preferable $I_{\mathrm{NWPC}} = I_0/\sqrt{2}$. That is why it is necessary to adjust to these requirements by multiplying NWPCs due to the variation of I_{NWPC}. It is feasible to resolve this problem by connecting a SuFET device to a number of parallel NWPCs. The number NWPCs should be calculated according to

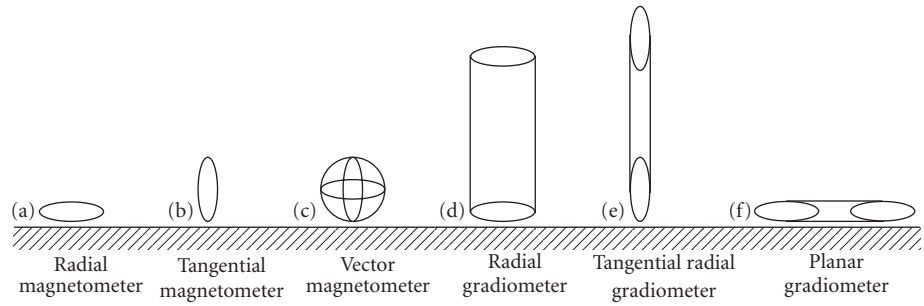

Figure 17: Flux transformer configurations for BEM applications. Reprinted with permission from [11], IOP Publishing Ltd. The shaded region represents the scalp surface. (a) Radial magnetometers measure radial or normal component of the MFs; (b) tangential magnetometers measure tangential components of MFs; (c) vector magnetometers determine the three orthogonal components at each location, measuring the vector MF; (d) radial gradiometers measure the radial gradient of radial field; (e) tangential radial gradiometers measure the radial gradient of tangential fields; (f) planar gradiometers measure tangential gradient of radial fields.

the maximum anticipated I_c for the particular application of SIM:

$$N_{\mathrm{NWPCs}} = \mathrm{Integer}\left(\frac{I_{\max}}{I_0}\right),$$
$$I_{\mathrm{NWPC}} \cdot N_{\mathrm{NWPCs}} \le I_{\max} \le I_{\mathrm{NWPC}} \cdot N_{\mathrm{NWPCs}}\sqrt{2}. \tag{14}$$

The n-NWPCs number of NWPCs should be commutated according to the I_c variations: adding additional coils when $I_c = I_0 \cdot X$ and rejecting one when $I_c < I_0 \cdot X$, where $X = 1, \ldots, N$ (Figure 18).

Switching output points $n1, \ldots, n$NWPCs can be defined analytically when I_c is legal to I_0 [27]:

$$V_{\mathrm{NWPC}}(X) = X\hbar\omega_T(Q_G)/2e \tag{15}$$

or experimentally when a high-frequency voltage component on the channel appears.

Finally, the transfer function in multi-NWPCs mode is defined as

$$G(X)_{\mathrm{SIM}} = \frac{A_{\mathrm{SIM}}}{\alpha_{\mathrm{SIM}}}\left(\frac{XI_0z_c}{jH} + \mu_0 S_{\mathrm{eq}}\omega\right) = G_{\mathrm{SIM}} + \frac{XI_0z_c}{H}\frac{A_{\mathrm{SIM}}}{\alpha_{\mathrm{SIM}}}. \tag{16}$$

For output voltage with an additional component V_{NWPC} which will arise on the drain-to-source resistor, we can write

$$V_{\mathrm{out}} - \frac{V_{\mathrm{NWPC}}}{2} = \frac{Q_G}{C} + \frac{\hbar\omega_T Q_G}{2e}\left(1 - \frac{\mu_0 S_{\mathrm{eq}}\omega H}{I_0 Z_c}\right). \tag{17}$$

Employing the same considerations we can obtain the transfer function of the second SIM operational mode when $I_{\mathrm{NWPC}} \ge I_0$:

$$\begin{aligned} G_{\mathrm{SIM}\,2} &= \frac{V_{\mathrm{GS}} - V_{\mathrm{DS}}/2}{H} \\ &= \frac{A_{\mathrm{SIM}}}{\alpha_{\mathrm{SIM}}}\left(\frac{I_0 z_c}{jH} + j\mu_0 S_{\mathrm{eq}}\omega\right) \\ &= G_{\mathrm{SIM}} + \frac{\hbar\omega_T(Q_G)}{2eH}. \end{aligned} \tag{18}$$

The main advantages of the NWPCs SIM with respect to the existing BM sensors are

(1) because their overall dimensions are not restricted by cooling volume, there is the opportunity to exploit NWPCs with different dimensions so as to reduce power consumption and mass of refrigeration installation;

(2) the dimensions of NWPCs are reduced and they are not shielded by cryogenic wrap. This absence of shielding enables better resolution and penetration when measuring;

(3) the NWPC is not constrained by cryogenic temperatures and may be extended a large distance from the electronic circuits in different working fluids;

(4) interaction between NWPCs and refrigeration systems is avoided as they are completely separated. The temperature variation of the cooling fluid does not influence sensor coils and the EM compatibility of the magnetometer is improved;

(5) it functions in two different modes depending on the ratio of the SuFET critical current to NWPC current;

(6) it functions in two different modes depending on the ratio of head coil's nanowire temperature to the critical temperature, current, and magnetic field of this wire;

(7) it is possible to mix the said modes during operation according to the requirements of measuring process;

(8) it is possible to multiply both NWPCs and SuFET-based circuits in order to match better magnetometer with its surrounding MF, or with measuring process.

5.2. BEM NMSC Employing NWPCS Arrays. A miniaturized niobium based DC SQUID magnetometer for high MF sensitivity applications has been developed. The sensing coil consists of an integrated square superconducting coil with a length of 3 mm, involving a device area much smaller with respect to the standard SQUID magnetometers with a comparable MF sensitivity; so it allows increasing the spatial resolution keeping the MF sensitivity unaltered [28]. Furthermore, a small PC minimizes its antenna gain,

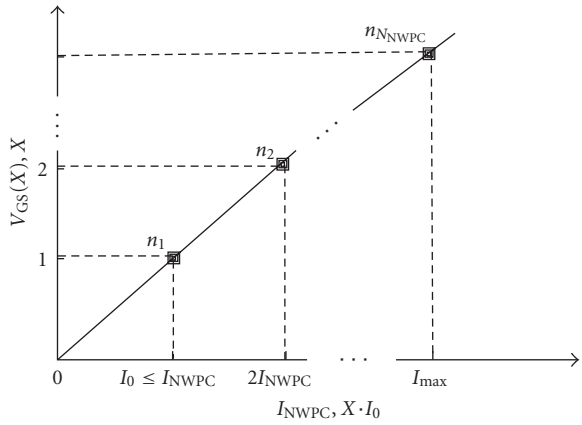

Figure 18: MultiNWPC operational mode of the SIM: discretizing of output voltage according to the steps of the NWPC I_c, or SuFET's channel critical I_0, current.

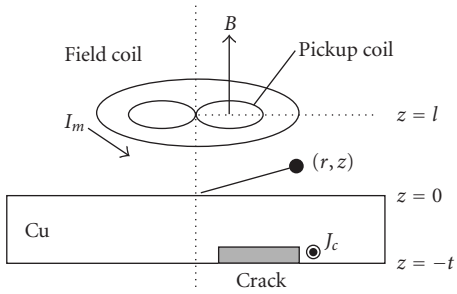

Figure 19: Geometry used in eddy current analysis. Reprinted with permission from [29].

reducing the radio frequency interference. At $T = 4.2$ K, the sensors have shown smooth and resonance free $V - \phi$ characteristics and an intrinsic white MF noise spectral density as low as $5.8\,\text{fT/Hz}^{1/2}$, measured in flux locked loop configuration. Due to their compactness and good characteristic parameters, such sensors are suitable for large multichannel systems used in BEM imaging.

A detection system for eddy current testing (ECT) utilizing a normal PC cooled at T_j 77 K and a picovoltmeter based on a high-T_c SQUID has been developed [29]. In this system, the PC is located in an unshielded environment, whereas the voltage across the coil is detected with the SQUID picovoltmeter placed in a small magnetic shield. It was shown that the coil could be moved in the unshielded environment without the degradation of its performance (Figure 19). By moving the coil, we successfully detected a small crack on the back surface of a Cu plate in an unshielded environment.

A new design for BM scanning or sounding nanomicroscope (NMSc) combines a simple mechanical arrangement with a miniature NW *exciting/PC (EC/PC)* of *SIM* [15]. The microwave imaging process (Figure 20) is shown on a prototype sample: a normal conducting ring of self-inductance L_i and resistance R_i. The quantity L_0 is the PC self-inductance and MI_i represents the magnetic coupling of

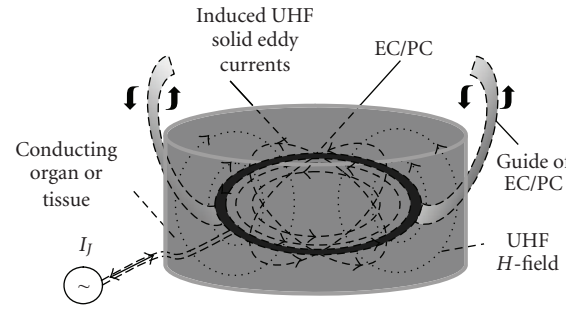

Figure 20: Schematic diagram of SIM based MNSC.

PC through a mutual inductance M to an external circuit carrying a current I_i in the material or tissue. If $\omega_T \gg R_i L_i$, then R_i may be ignored and $I_i(\omega_T) \approx -I_j(\omega_T)M/L_i$.

An interesting structure is that of helical carbon nanotubes (CNTs), or nanocoils for EC/PC (Figure 21(a)). Nanocoils offer unique electronic properties that straight CNTs do not have. The plasticity of CNTs will be relevant to their use in nanoscale devices [30].

For nonzero drain voltages, the SuFET absorbs low-frequency power of the average Josphson current I_J and reemits this power at extremely high frequencies. The feasibility of the transistor function on a yarn-like structure has been demonstrated (Figure 21(b)) [31]. As a result, the decreasing of the SuFET channel's current is defined by the value of losses for eddy currents $I_i(\omega_T)$ in the tissue:

$$\Delta I_J(\omega_T) = I_J(\omega_T) - I_i(\omega_T) = K_J\left(\frac{V_{DS}}{2} - V_{GS}\right)\left(1 - \frac{M}{L_i}\right). \tag{19}$$

Thus, by monitoring the change in $\Delta I_j(\omega_T)$ as a function of PC position, we make use of the factor M/L_i dynamics of the tissue to obtain a micro- or nanowave screening image.

One-dimensional nanowires are destined to play an important role in FETs and their potential applications in various fields [32]. Among these materials, ZnO nanowires have been intensively investigated because of their simple synthetic procedure and high crystalline quality. Recently, flexible and transparent substrates have gained increasing attention in the semiconductor industry, due to their lightweight and the facility they provide for fabricating electronic devices.

Hence the mechanical stability of the smart textiles is sufficient for implantation of the planar structures (Figure 22). Since the developed system allows the micro- and nanoscopic of room and tissue temperature samples, such testing will be of practical use for clinical diagnostic.

To achieve a high spatial resolution, our NMSC uses a small ambient temperature NWPC(s) directly as a magnetic sensor, rather than a SQUID's pickup loop coupled to a cooled SuFET. Sounding and scanning closer to the tissue improve the spatial resolution, thanks to the complete penetration into the measuring process. Other than the SuFET itself, there are no other microwave components, sources, or detectors. This is particular advantageous at very high frequencies where components are difficult to

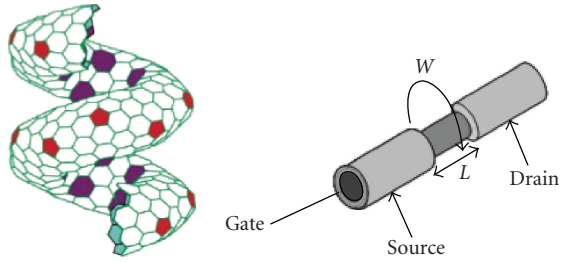

(a) (b)

Figure 21: Application of the NW and polymer elements, (a) a helical CNT tube (Reprinted with permission from [30]); (b) an e-yarn (reprinted with permission from [31]). Copyright 2006, American Institute of Physics.

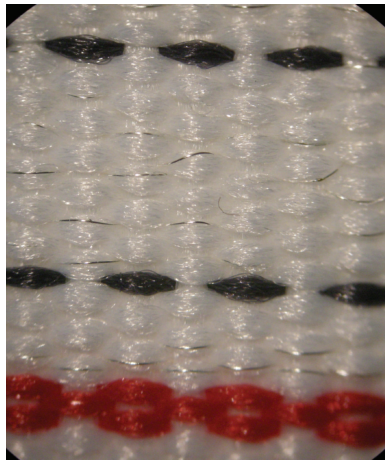

(a)

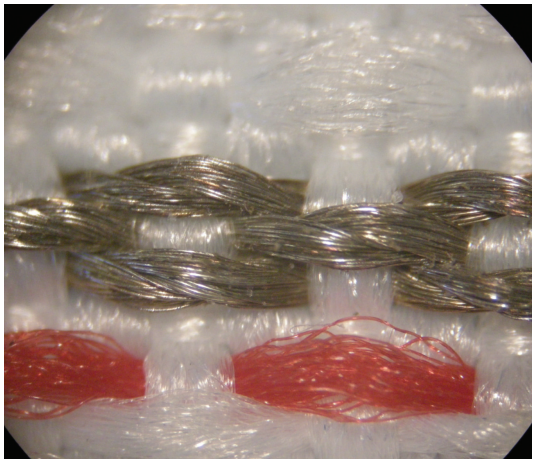

(b)

Figure 22: A variety of conductive textile ribbons and elastics have been developed. Reprinted with permission of Ohmatex ApS.

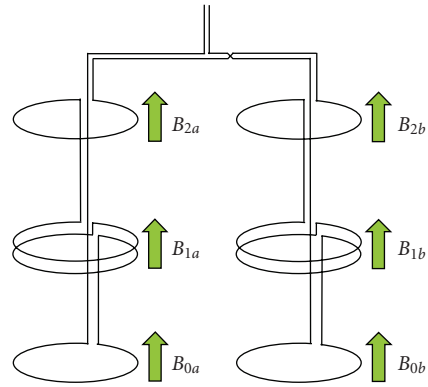

Figure 23: NWEC/PC for "two-dimensional" gradiometer that detects both axial-second-order gradient and planar-first-order gradient of MF. Reprinted with permission from [26].

construct. In conclusion, we note that the ability to detect small regions of nonmagnetic conducting materials, gives the magnetic flux NMSC broad capabilities in material analysis.

Conventional gradiometers, such as wire-wound, thin-film, or electronic gradiometers, are axial or planar, that is, "one-dimensional" that detects the gradient of an MF in one direction. These one-dimensional gradiometers effectively reduce the ambient MF as their order increases. However, they also reduce the BEM signal. A "two-dimensional" gradiometer detects the gradient of an MF in two orthogonal directions to achieve high SNR [26]. It focuses on a two-dimensional gradiometer that detects both the axial-second-order and planar-first-order gradients of an MF. Figure 23 shows EC/PC for the two-dimensional gradiometer.

The described NMSC is suitable for investigating both the structure of synthetic and organic objects, and their comparing analysis (see Table 1). Following the strings of the table, investigations of biological surfaces are performing according to the surface integrals for an NMSC modulus. The same is applying to the investigations of the volumes V_1 and V_2 as the double and triple integrals, respectively.

With advances in spatial resolution reaching the atomic scale, two-dimensional (2D) and 3D imaging in electron microscopy has become an essential methodology in various fields of study. A 4D imaging, with in situ spatiotemporal resolutions, in ultrafast electron microscopy (UEM) has been reported [33]. The ability to capture selected-area-image dynamics with pixel resolution and to control the time separation between pulses for temporal cooling of the specimen made possible studies of fleeting structures and morphologies by NMSC.

Table 1: Dependence of the received structure parameters on the functioning mode of NMSC and possible bounds for spreading of the said method.

Object	Mode	
	Modulus	Gradient
Surface	$I_2 = \iint_S f(x, y, z)dx\,dy$	$\Delta I_2 = I_2' - I_2''$
Volume	$V_2 = \iiint_V f(x, y, z)dv$	$\Delta V_2 = V_2' - V_2''$
Structure level	Inside structure of the objects	Differential investigation of the twin (pair) objects
Object level	Inhomogeneous structure	Differential investigation of the inhomogeneous twin (pair) objects.

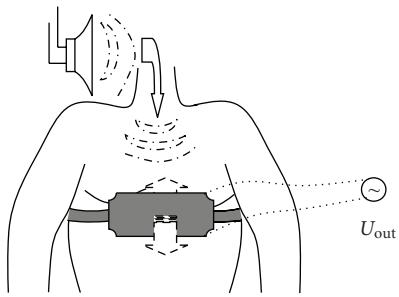

Figure 24: Vibration of a membrane placed on a chest.

A nanoSuFET with a high-temperature superconducting channel is introduced into the tissue or material for transducing their signals in both directions. The microwave imaging process is based on the nanowire or CNT EC/PC. The equation for computations of the coils' RLC values on UHF are presented. The sensitivity of this nano-microscope can be estimated as $H_J = 10^{-4}\,(\text{A}\cdot\text{m}/\sqrt{\text{Hz}})$ with SNR equal to 10^4. The sensitivity of an advanced first-order biogradiometer is equal to 3 fT/$\sqrt{\text{Hz}}$. The smallest change in magnetic moment detected by this system in the band 10 Hz is 1 fJ/T.

5.3. Biotransducer of the Acoustical Flow. Pulmonography is an acoustical method of local investigation of the lungs by registration of changes in different places of a chest wall (Figure 24).

In order to achieve acoustic analysis of speech signals, a method for detection of the position in a coordinate system of the tongue using a small magnetic rod on the tongue surface and the sensor unit is developed, which is set in the vicinity of the mandible or cheek. In order to determine the coordinate position of the magnetic rod, two sensors are necessary [34].

Another example of the use of the magnetic sensing method in the measurement of the mandible and other organs by an AC MF employing transmitting and receiving coil pairs [35] is provided. A computer on-line method for measuring articulatory activities is presented. Small receivers are attached to articulatory organs, recording their motion via electric voltages induced by external inhomogeneous EM fields. The signals, which are the electrical equivalents of the motion relative to a coordinate system, are subjected to automatic computer analysis. Experiments have been performed and the results for some utterances are shown, demonstrating the abilities of the system. Moreover, as an example of automatic performance, lip-opening data are deduced.

An EM contactless excitation principle was presented to induce mechanical vibrations on miniaturized electrically conductive resonant structures to be used as passive sensors. An external coil arrangement generates a time-varying MF which induces eddy currents on the structure surface. The interaction between the eddy currents and MF causes forces which can set the structure into vibration. The principle avoids any contact to the resonator structure to inject current and only requires the structure to be electrically conductive, without the need for specific magnetic properties. The principle is attractive for the development of passive sensors operating in environments with limited accessibility or incompatible with active electronics [36].

Realization of our innovation is proposed by the use of ambient natural MF which regards DC or stationary [37]. The employed PCs for creating and/or receiving of MF are made from the superconducting material. As a result, the hard magnet of an electrodynamical transducer is replaced by the natural MF, and Meissner effect displaces this MF from any superconductor PC or continuous section, because any change of the ambient MF vortical currents arises in a superconductor which compensates for these changes, according to the Lenz law.

Some merits of this method reside in reducing the device's mass and energy consumption due to functioning in the passive mode. It is that a superconducting membrane is oscillating into the ambient MF. In such arrangement, the sensitivity of transducing of the acoustical signal into electrical one is rising. Because, of the virtual absence of noises in the superconducting element.

Electro-acoustical device provides the transducing of the membrane oscillations in an electrical current I and in reverse to acoustical wave (Figure 25). During this transducing a value of PC's I is defined by

$$I = \frac{\mu_0\mu_{\text{ef}}W\pi d^2}{4L}H = \frac{BW\pi d^2}{4L}, \tag{20}$$

where $W$is total turn number of solenoid.

On the conductor with a current I in MF, B is affecting the force:

$$F = BlI. \tag{21}$$

The ratio of this force to a plane of a surface of membrane S gives a pressure of an acoustical wave on the membrane or,

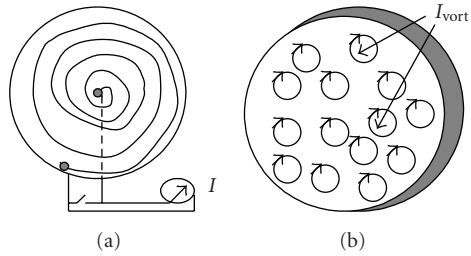

Figure 25: The acoustical membrane with the implanted NWPC: (a) made from a superconducting material, (b) with the vortical currents.

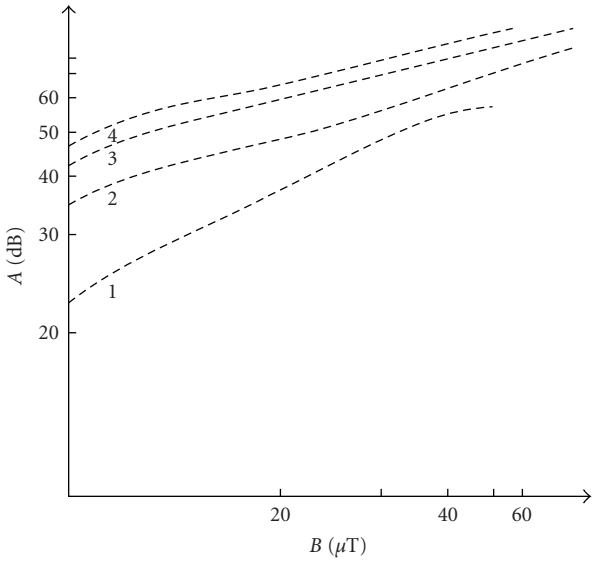

Figure 26: A graph of dependence between the acoustical intensity A and MF B for different effective areas of PCs. 1: $W = 5 \cdot 10^3$; 2: $W = 10^4$; 3: $W = 15 \cdot 10^3$; 4: $W = 2 \cdot 10^4$.

in reverse, the value of acoustical pressure of the membrane:

$$p = \frac{BlI}{S} = \frac{B^2 lW\pi d^2}{4LS}\,[\mathrm{H/m^2}]. \tag{22}$$

Taking into account the standard threshold sound pressure $p_0 = 2 \cdot 10^{-5}$ Pa, the absolute value of a sound pressure is defined as

$$A = 20lg\frac{B^2 lW\pi d^2}{4LSp_0}. \tag{23}$$

The second advanced mechanism for generation of the acoustic oscillations is using of Meissner effect, which is implemented by closed contact of a superconducting PC (Figure 25(a)), during the rising of vortical currents I_{vort} in the plane of the superconducting membrane (Figure 25(b)).

Figure 26 presents the dependence A from B in the earth MF for the value parameter's: $d = 0.2$ m, $L = 0.2$ H, $S = 0.04$ m^2. Suppling of a signal into the membrane and its picking up are carried out by SuFET. A linear dependence between an amplitude of oscillation A of the membrane and I of NWPC examines to the value I which is equal to the critical current I_0 of a superconductor. After reaching this level, the current I_0, and respectively also the transducing ability, is significantly decreasing due to going of a (high-T_c) superconductor into the resistive state.

6. Results. The Design Variants of NWPCs

The variety of applications of the novel superconducting, organic and CNT FETs with NWPCs allows us to design transducers of BSs (electronic, nerve, DNA, etc.). They transduce BSs into different quantities, including electric voltage, and the density of chemical and biomolecules. On the other hand, the said BSs can be controlled by the applied electrical signals, or bio and chemical mediums.

The described SuFET based sensors/transducers (SuFETTrs) designed on the basis of organic and nano SuFETs are suitable for describing the wide range of BS dynamical parameters (see Table 2). The table illustrates that a serial connection of the external NWPCs allows us to gain some integrated signal. The whole sensing or electronic control or nerve impulse (NI) spreads along the number of axons of the nerve fibre, the amount of ions passing through the NWPCs and the generalized BS passing through one or both spirals of DNA. When SuFET channel(s) are implanted into the tissue or process, we can acquire more precise data about the frequency distribution of NIs, volume distribution of ionized molecules and detecting activity of individual nucleotides.

The preliminary calculations confirm the possibility of broadening the SuFETTr's action from MF to the biochemical medium of the BSs [13]. The main parameters of these BSs can be gained by applying the arrangement of the SuFETTr(s) to the whole measurement system. Dual directional function of SuFETTr enables decoding of the BS by comparing the result of its action on some process or organ, by using a simulated electrical or biochemical signal after reverse transducing through the SuFETTr(s). Furthermore, this decoded signal will provide a basis for creating feedback and feedforward loops in the measuring system for more precize and complete influence on the biochemical process.

The described biosusceptometer or nano-microscope is designed on the basis that EMTMs are suitable for investigating both the structure of organic objects and comparing analysis (see Table 3). The strings of the table illustrate, that investigations of biological surfaces are performing according to the surface integrals for a biosusceptometer and nano-microscope moduluses, respectively. The surface gradients are being acquired by finding the difference between the respective values of I_1 or I_2. The same is applied to the investigations of biological volumes V_1 and V_2 as the double and triple integrals, respectively. The next two strings are explaining the bounds on the possible spreading of the said method.

Exploitation of the parallel input to SuFETTr allows determination of space and time dynamics of BSs in the nerve fibre and neuronic synapse, also the amplification of the output signal U_{out} by multiplying the concentration of molecules according to a number of input BSs. After the

Table 2: Dependence of the received BS parameters on the mode of SuFETTr's functioning.

Medium	Mode			
	Serial		Parallel	
	External	Implantable	External	Implantable
NI	$\int i_{\text{bio}} = 1$ contr. or sens. impuls.	$i_{\text{bio}} = i_{\text{bio}}(f_1) + i_{\text{bio}}(f_2) + \cdots + i_{\text{bio}}(f_N)$	di_{bio}/dt, di_{bio}/dx	$\sum i_{\text{bio}} = 1$ network or 1 fibre
Molecules	$\int$ BSs $\rightarrow$ bio and chem. molec.	Variation of BSs $\rightarrow$ concentr. of molec.	$\sum$ BSs = 1 type of molec.	$\sum$ BSs = $\sum$ bio and chem. molec.
DNA	Propagation of BS along DNA's spirals	Decoding the BSs of nucleoted recognition	Space and length dynamic on both spirals	4 nucleoteds $\rightarrow$ 4 outputs

Table 3: Dependence of the received structure parameters on the mode of functioning—a biosusceptometer or nano-microscope.

Object	Device			
	Biosusceptometer modulus	Nano-microscope modulus	Biosusceptometer gradient	Nano-microscope gradient
Surface	$I_1 = \iint_S f(x,y,z)ds$	$I_2 = \iint_S f(x,y,z)dx\,dy$	$\Delta I_1 = I_1' - I_1''$	$\Delta I_2 = I_2' - I_2''$
Volume	$V_1 = \iint_S f(x,y)dx\,dy$	$V_2 = \iiint_V f(x,y,z)dv$	$\Delta V_1 = V_1' - V_1''$	$\Delta V_2 = V_2' - V_2''$
Structure level	Investigation of sheath (envelopes) of organs	Investigation of the inside structure of the organs and tissues	Comparing investigation of the organ's or tissue's areas	Differential investigation of the twin (pair) organs or tissues
Object (body) level	Investigation of homogeneous organs or tissues	Investigation of inhomogeneous organs or tissues	Comparing investigation of the homogeneous organ's or tissue's areas	Differential investigation of the inhomogeneous twin (pair) organs or tissues

implantation of parallel SuFET(s), the averaging or summation of this dynamic among the whole neural network, nerve fibre or neuronic synapse(s) is possible.

7. Conclusions

The invented nano-bio-transducer has the following fundamental improvements upon existing ones:

(a) the sign of the output voltage permits the determination of the direction of the input bioflow passing through a single SuFET device;

(b) situating the reference electrode outside the living organism makes precise measurement possible;

(c) the capability to regulate the proportion of axons, neurons, or flows that are being investigated to the untouched ones—either the whole cross section of the fibre or flow, or any part of them is realized;

(d) the possibility to substitute the SuFET device or to adjust its ratings to comply with the conditions of the measurement process without repeatedly destroying nerve fibre or flow vessel is realized;

(e) the transducer could create conversion in both directions, respectively in passive and active modes;

(f) the combination of biocompatibility and tissue equivalence in both the diamond and protein-based (organic) FETs makes them naturally fit for implantation;

(g) the possibility to compose a converging device by changing the instrument—from a current sensor to biosusceptometer, from a flowmeter to nano-microscope, and so forth—by switching-over (modifying) of SuFET's working mode or transferring from the natural ambient conditions to applying of the exciting MF is realized .

The reviewed variety of FETs shows the varying extent of readiness for them to be exploited in SuFETTr of BSs. The most appropriate for such an application are the ordinary solid-state SuFET modifications and novel CNT based SuFETs. The organic SuFETs are not amply developed, but this work is being carried out in a number of directions. At the same time, the NWPCs, which are necessary for the external sensor with respect to the transducing medium (solid-state conductor, nerve fibre, flow of ions, and DNA spiral), and corresponding low-ohmic wire traces for connecting NWPCs to the FET's channel are sufficiently developed, even at nano dimensions.

The preliminary calculations confirm the possibility of broadening the SuFETTr's action from magnetic field to

Table 4: Measuring effects (values) and the relative nano-bio-sensors (for interfacing).

Physical value	NW element			
	SuFET channel	PC(s)	EC	Superconducting membraine
Ionic currents	NI_{impl}	NI_{ext}	NI_{contr}	NI_{impl}
FE/FEM	EMTM	EMTM	EMTM	Acoustical EMTM
Magnetic induction	NI_{contr}	SIM	NMSc	Noise absorb.
MHD/MGD	Gaseous FM	Volume FM	Active FM	Acoustical FM
Acoustical oscillations	—	Acoustical transducer	Loudspeaker	transd. and loudspeak.

Table 5: Geometrical form of the distributed in space and time arrays.

Dimension	Value			
	Scalar	Scalar array	Vector	Tensor
Point	module	differential	triaxial	triaxial vector
Line	gradiometrical	differential gradiometrical	differential triaxial	differential triaxial vector
Curve	differential module	gradiometrical module	differential triaxial	differential triaxial vector
Plane	gradiometrical module	gradiometrical differential module	gradiometrical triaxial	gradiometrical triaxial vector

the biochemical medium of BSs. The main parameters of such BSs can be gained by applying the arrangement of the SuFETTr(s) to the whole measurement system. Two directions of SuFETTr function enable decoding of the BS by comparing the result of its action on some process or organ with an action on them of the simulated electrical or biochemical signal after their reverse transducing through the SuFETTr(s). Furthermore, this decoded signal will provide a basis for creating feedback and feedforward loops in the measuring system for more precise and complete influence on the biochemical process.

Performances of compact fully integrated SQUID magnetometers, recently developed, have been investigated in view of their employment in large multichannel systems for BM imaging. The performance study has been consisted in the computation of the magnetic responses to a current dipole which is the most fundamental approach used in BM [29].

In SQUID magnetometers used to measure biomagnetic fields, PCs are usually arranged in a gradiometric configuration to reduce environmental MF noise. The direct-feedback gradiometer does not need superconductive wires between the two PCs. The feedback coils can be connected with a normal conductive wire and an axial gradiometer made of thin films without any superconducting contacts [30]. In clinical applications, it is important to measure the signals from several points at the same time.

BM measurements can sensitively and noninvasively be used to detect a BM signal from the myocardium or nerve. NWPCs of wire-wound gradiometers are wound in opposition and balanced so that a uniform field can link the zero net flux. Thin-film gradiometers are better than the others in terms of gradiometric balance. A two-dimensional gradiometer that detects the gradient of an MF in two orthogonal directions to measure the biomagnetic signal in an unshielded environment is developed. The developed gradiometer is based on a low-T_c SQUID and wire-wound PC, and detects both the axial-second-order and planar-first-order gradients of MF [31].

A number of both active and passive electronic elements are used with nanowires. On the other hand, any particular element is susceptible by the effect of some specific physical quantity. The relevant sensing devices which are acquired on the said bases are shown in Table 4. As a result, a wide range of the nano-bio-sensors allow both measuring the variety of ionized biosignals and interfacing the bioEM signals with further stages of electronic systems.

The designed sensors are arranged in a space and time arrays for investigation of the biostructures of the different level of precision. In Table 5, the geometrical dimensions from a point to volume ranges are transformed to the mathematical terms. This correspondence is established by composing the head sensors from Table 4 into the various gradiometry schemes, from a simple planar to the 2d vector enclosing.

The advance in the instrumentation techniques and technology of materials allows introducing of more accurate methods of breath diagnostics and sensors for their execution. At this level of progress, the head sensors of paramount sensitivity and simplicity in picking up are functioning with minimal changes of the physical variables. The ambient MFs of the wide frequency range are present in

any point of the human being which makes them suitable for using as body-sounding.

The recent breakthrough in superconducting and nanotechnologies caused to creation of ISs which have better informational capability in some diagnostical purposes. These devices are based on the universal law of the EM induction on the one hand and different special effects of MF interaction with a medium on the other.

Part of the described transducing principles and the respective sensors are noninvasive. That is why diagnostics of breath characteristics can be performed in complex arbitrary of their combinations, (i.e., simultaneously for necessary body parts and repeatedly during the period of observation). In such way a more complete investigation will be accomplished within the scope of the known methods of breath diagnostics and opportunities for new ones are opening.

Since the proposed variety of bio-nano-sensors are passive, they do not affect the functions of the organs and their interaction. Safety for the acquired diagnostical facilities is applicable for both clinical and in home care situations.

References

[1] R. Kanada, L. Pan, S. Akita, N. Okazaki, K. Hirahara, and Y. Nakayama, "Synthesis of multiwalled carbon nanocoils using codeposited thin film of Fe-Sn as catalyst," *Japanese Journal of Applied Physics*, vol. 47, no. 4, pp. 1949–1951, 2008.

[2] Yu. Fujiyama, R. Tomokane, K. Tanaka, et al., "Alignment of carbon nanocoils in polymer matrix using dielectrophoresis," *Japanese Journal of Applied Physics*, vol. 47, no. 4, pp. 1991–1993, 2008.

[3] J. Hobden, "Self assembled molecular nanowires: electronic properties," *Nano Today*, vol. 3, no. 5-6, p. 11, 2008.

[4] S. A. Fortuna and X. Li, "GaAs MESFET with a high-mobility self-assembled planar nanowire channel," *IEEE Electron Device Letters*, vol. 30, no. 6, pp. 593–595, 2009.

[5] J. Shui and J. C. M. Li, "Platinum nanowires produced by electrospinning," *Nano Letters*, vol. 9, no. 4, pp. 1307–1314, 2009.

[6] T. Katsura, Ya. Yamamoto, K. Maehashi, Y. Ohno, and K. Matsumoto, "High-performance carbon nanotube field-effect transistors with local electrolyte gates," *Japanese Journal of Applied Physics*, vol. 47, no. 4, pp. 2060–2063, 2008.

[7] Yu. Lu, S. Bangsaruntip, X. Wang, L. Zhang, Y. Nishi, and H. Dai, "DNA functionalization of carbon nanotubes for ultrathin atomic layer deposition of high κ dielectrics for nanotube transistors with 60 mV/decade switching," *Journal of the American Chemical Society*, vol. 128, no. 11, pp. 3518–3519, 2006.

[8] K.-I. Ogawa, N. Aoki, K. Miyazawa, et al., "C60 nanowhisker field-effect-transistor application for nano-electronics," *Japanese Journal of Applied Physics*, vol. 47, no. 1, pp. 501–504, 2008.

[9] N. Misra, J. A. Martinez, S.-C. J. Huang, et al., "Bioelectronic silicon nanowire devices using functional membrane proteins," *Proceedings of the National Academy of Sciences of the United States of America*, vol. 106, no. 33, pp. 13780–13784, 2009.

[10] W. Yang, P. Thordarson, J. J. Gooding, S. P. Ringer, and F. Braet, "Carbon nanotubes for biological and biomedical applications," *Nanotechnology*, vol. 18, no. 41, Article ID 412001, 12 pages, 2007.

[11] J. Vrba and S. E. Robinson, "SQUID sensor array configurations for magnetoencephalography applications," *Superconducting Science and Technology*, vol. 15, no. 9, pp. R51–R89, 2002.

[12] R. Sklyar, "Superconducting organic and CNT FETs as a biochemical transducer," in *Proceedings of the 14th International Symposium on Measurement and Control in Robotics (ISMCR '04)*, p. 113, NASA Johnson Space Center, Houston, Tex, USA, September 2004, section 24.

[13] R. Sklyar, "Sensors with a bioelectronic connection," *IEEE Sensors Journal*, vol. 7, no. 5, pp. 835–841, 2007.

[14] L. E. Fong, J. R. Holzer, K. K. McBride, E. A. Lima, F. Baudenbacher, and M. Radparvar, "High-resolution room-temperature sample scanning superconducting quantum interference device microscope configurable for geological and biomagnetic applications," *Review of Scientific Instruments*, vol. 76, no. 5, Article ID 053703, 9 pages, 2005.

[15] R. Sklyar, "A SuFET based sensor for nano-microscope," *Journal of Automation, Mobile Robotics and Intelligent Systems*, vol. 1, no. 3, pp. 3–20, 2007.

[16] G. P. Chatzimavroudis, "Blood flow measurements with magnetic resonance phase velocity mapping," *Measurement*, vol. 37, no. 3, pp. 201–212, 2005.

[17] R. Sklyar, "The microfluidic sensors of liquids, gases, and tissues," *Journal of Automation, Mobile Robotics and Intelligent Systems*, vol. 1, no. 2, pp. 20–34, 2007.

[18] M. Hajjhassan, V. Chodavarapu, and S. Musallam, "Neuro MEMS: neural probe microtechnologies," *Sensors*, vol. 8, pp. 6704–6726, 2008.

[19] R. Sklyar, "CNT and organic FETs based two-way transducing of the neurosignals," in *Nanotechnology 2008: Life Sciences, Medicine, and Bio Materials*, vol. 2, chapter 6: Nano Medicine & Neurology, pp. 475–478, Nano Science & Technology Institute, CRC Press, Cambridge, Mass, USA, 2008.

[20] R. Sklyar, "Direct processing of the MCG and MEG signals," in *Proceedings of the 6th International Conference on Biomedical Applications of Nanotechnology*, p. 2, Charite, Berlin, Germany, March 2009.

[21] R. Sklyar, "Analytical treatment of the signal propagation in an EM transistor/memristor (EMTM)," in *Proceedings of the 2nd International Workshop on Nonlinear Dynamics and Synchronization (INDS '09)*, pp. 116–120, Klagenfurt, Austria, July 2009.

[22] J. Borghetti, Zh. Li, J. Straznicky, et al., "A hybrid nanomemristor/transistor logic circuit capable of self-programming," *Proceedings of the National Academy of Sciences of the United States of America*, vol. 106, no. 6, pp. 1699–1703, 2009.

[23] G. S. Snider and R. S. Williams, "Nano/CMOS architectures using a field-programmable nanowire interconnect," *Nanotechnology*, vol. 18, no. 3, Article ID 035204, 11 pages, 2007.

[24] Ch. Hilty, E. E. McDonnell, J. Granwehr, K. L. Pierce, S.-I. Han, and A. Pines, "Microfluidic gas-flow profiling using remote-detection NMR," *Proceedings of the National Academy of Sciences of the United States of America*, vol. 102, no. 42, pp. 14960–14963, 2005.

[25] N. Sinha and J. T.-W. Yeow, "Carbon nanotubes for biomedical applications," *IEEE Transactions on Nanobioscience*, vol. 4, no. 2, pp. 180–195, 2005.

[26] Yu. Seki and A. Kandori, "Two-dimensional gradiometer," *Japanese Journal of Applied Physics*, vol. 46, no. 6, pp. 3397–3401, 2007.

[27] R. Sklyar, "Superconducting induction magnetometer," *IEEE Sensors Journal*, vol. 6, no. 2, pp. 357–364, 2006.

[28] C. Granata, A. Vettoliere, and M. Russo, "Miniaturized superconducting quantum interference magnetometers for high sensitivity applications," *Applied Physics Letters*, vol. 91, no. 12, Article ID 122509, 3 pages, 2007.

[29] K. Yao, T. Q. Yang, D. Yamasaki, K. Tazoh, and K. Enpuku, "Eddy current testing utilizing cooled normal pickup coil and superconducting quantum interference device picovoltmeter: comparison between experiment and analysis," *Japanese Journal of Applied Physics*, vol. 45, no. 6, pp. 4994–4999, 2006.

[30] Yo. Nakayama, "Plasticity of carbon nanotubes: aiming at their use in nanosized devices," *Japanese Journal of Applied Physics*, vol. 46, no. 8, pp. 5005–5014, 2007.

[31] M. Maccioni, E. Orgiu, P. Cosseddu, S. Locci, and A. Bonfiglio, "Towards the textile transistor: assembly and characterization of an organic field effect transistor with a cylindrical geometry," *Applied Physics Letters*, vol. 89, no. 14, Article ID 143515, 2006.

[32] J. Kang, K. Keem, D.-Y. Jeong, and S. Kim, "Electrical characteristics of ZnO nanowire-based field-effect transistors on flexible plastic substrates," *Japanese Journal of Applied Physics*, vol. 46, no. 9, pp. 6227–6229, 2007.

[33] B. Barwick, H. S. Park, O.-H. Kwon, J. S. Baskin, and A. H. Zewail, "4D imaging of transient structures and morphologies in ultrafast electron microscopy," *Science*, vol. 322, no. 5905, pp. 1227–1231, 2008.

[34] Y. Sonoda, "Magnetic sensors and medical bio-technology—measuring vibrations, displacements, and articulatory movements," *IEEE Translation Journal on Magnetics in Japan*, vol. 7, no. 9, pp. 714–721, 1992.

[35] G. van der Giet, "Computer controlled method for measuring articulatory activities," *Journal of the Acoustical Society of America*, vol. 61, no. 4, pp. 1072–1076, 1977.

[36] M. Baù, V. Ferrari, D. Marioli, E. Sardini, M. Serpelloni, and A. Taroni, "Contactless electromagnetic excitation of resonant sensors made of conductive miniaturized structures," *Sensors and Actuators A*, vol. 148, no. 1, pp. 44–50, 2008.

[37] R. Sklyar, "The method of receiving and generating of the acoustical oscillations and transducing devices of this oscillations on its bases-electrodynamical, noise absorbtional, and magnetometrical," UA patent no. 74533, bulletin 1, 7 pages, 2006.